

Spin polarization tuning in $\text{Mn}_x\text{Fe}_{1-x}\text{Ge}_3$

A. Stroppa and G. Kresse

Faculty of Physics, University of Vienna,

and Center for Computational Materials Science,

Universität Wien, Sensengasse 8/12, A-1090 Wien, Austria

A. Continenza

CNISM- Dipartimento di Fisica Università degli

Studi dell'Aquila, Via Vetoio 10 L'Aquila, Italy;

Abstract

Experimentally, the intermetallic compound Mn_4FeGe_3 has been recently shown to exhibit enhanced magnetic properties and spin polarization compared to the Mn_5Ge_3 parent compound. The present *ab-initio* study focusses on the effect of Fe substitution on the electronic and magnetic properties of the compound. Our calculations reveal that the changes on the Fermi surface of the doped compound are remarkable and provide explanations for the enhanced spin-polarization observed. Finally, we show that it is indeed possible to tune the degree of spin-polarization upon Fe doping, thus making the $\text{Mn}_{1-x}\text{Fe}_x\text{Ge}_3$ intermetallic alloy very promising for future spintronic applications.

PACS numbers: 71.15.Mb;71.20.Lp; 72.25.Ba; 72.25.Hg

The ferromagnetic intermetallic Mn_5Ge_3 compound is a very promising spin injector: it can be easily grown epitaxially on the Ge(111) substrate[1, 2, 3] and can provide spin-polarization of about 42 % while preserving ferromagnetic ordering up to a Curie temperature (T_C) as high as 296 K. Very recently, T. Y. Chen *et al.* have shown that replacing one Mn atom/f.u. with Fe may lead to a remarkable effect on the spin-injection properties.[4] This immediately opened the possibility for *Spin Polarization Engineering* (SPE) of Mn_5Ge_3 by means of Fe doping. The reasons for the remarkable spin polarization enhancement in Mn_4FeGe_3 are not clear yet and await theoretical explanations.

Density Functional calculations were performed using the VASP package within the Generalized Gradient Approximation (PBE-GGA).[8] PAW pseudopotentials[9, 10] were used for both Ge and TM-atoms: the semicore $3p$ states are considered as valence (core) for Mn (Fe); the $3d$ states are frozen in the core for Ge. The kinetic energy cutoff used for the wave functions was fixed to 350 eV. (4,4,6) Γ -centered k -points were used for the self-consistent cycle, while a (12,12,14) k -point grid was used for the calculation of the Fermi velocity. All the atomic internal positions as well as the volume and shape of the unit cell were relaxed minimizing the *ab-initio* stress and forces.

The Mn_4FeGe_3 compound can be represented as a solid solution of Fe in Mn_5Ge_3 , *i.e.* $\text{Mn}_{5-x}\text{Fe}_x\text{Ge}_3$ with $x = 1$. For $x = 0$, at ambient conditions, Mn_5Ge_3 crystallizes in the hexagonal $D8_8$ type (space group $P6_3/mcm$) with a unit cell containing 16 atoms: 10 Mn atoms in two inequivalent sites identified using the Wyckoff notation [$4M_I$ in $4(d)$; $6M_{II}$ in $6(g)$] and 6 Ge atoms in $6(g)$ sites. The description of the crystal structure has been given elsewhere.[11] For $x = 5$, Fe_5Ge_3 is also hexagonal but belongs to the $D8_2$ symmetry type (space group $P6_3/mmc$), so that the mutual solubility of the end members could be limited by their different crystal structure. The limit of solubility appears to occur at $x=1$, or slightly beyond,[5] resulting in the Mn_4FeGe_3 compound that still preserves the same crystal structure as Mn_5Ge_3 . Therefore, Mn_4FeGe_3 can be described using an ordered supercell containing 16 atoms, *i.e.* 8 Mn, 2 Fe and 6 Ge atoms.

We start our study considering one Fe atom at both the M_I or M_{II} site, and we found that Fe prefers to occupy the M_I site with an energy gain of 280 meV/cell with respect to the M_{II} site: thus, in agreement with experiments,[5, 6, 7] the smaller and less electropositive iron atom substitutes preferentially Mn on the $4(d)$ sites.[12] This not unexpected since occupation of the M_I site allows the metallic atoms to be closer[13], consistently with the Fe

TABLE I: Structural data (lattice constant a and c/a ratio, magnetic moments and heat of formation) for the structures considered compared with experiments where available.

System	$a(\text{\AA})$	c/a	$\mu_{M_I} (\mu_B)$	$\mu_{M_{II}} (\mu_B)$	$\mu_{Ge} (\mu_B)$	$\mu_T (\mu_B/\text{f.u.})$	$\Delta H_f(\text{eV}/\text{atom})$
Mn ₅ Ge ₃	7.142	0.697	2.22	3.11	-0.16	2.70	-0.140
Exp[13]	7.184	0.703	1.96	3.23		2.60	
Mn ₄ FeGe ₃	7.134	0.690	1.75 (Fe), 2.35 (Mn)	3.05	-0.15	2.59	-0.145
Exp[4]	7.184	0.696				2.35	
Exp[7]	7.138	0.702	1.55	2.45		2.10	
Fe ₅ Ge ₃	6.967	0.692	1.58	2.17	-0.11	1.85	-0.061

atoms having smaller atomic radius than Mn. The 4(d) atomic positions (in internal coordinates) lie in two different planes along the hexagonal c -axis: $(1/3, 2/3, 1/2)$, $(2/3, 1/3, 1/2)$, $(1/3, 2/3, 0)$, $(2/3, 1/3, 0)$ and they can be occupied by two iron atoms in three different and non-equivalent configurations. We find that, in the lowest-energy state, the Fe atoms are located on the sites belonging to the $z = 0$ or $z = c/2$ symmetry equivalent planes.

In table I, we show the calculated lattice constants and magnetic moments of Mn₅Ge₃, Mn₄FeGe₃ and the hypothetical Fe₅Ge₃ compound in the D_{8h} crystal structure. The formation energy (ΔH_f) is defined with respect to reservoirs of atoms in the pure bulk phases γ -Mn AFM1, FM bcc-Fe and diamond Ge; we have chosen the sign in such a way that stable compounds have negative formation energies. For Mn₅Ge₃, the theoretical lattice constants a and c are slightly underestimated with respect to the experimental values (0.5 % and 1.4 %, respectively). The calculated magnetic moments correctly reproduce the relative magnitude of the M_I and M_{II} moments, with the former carrying smaller moments, in agreement with experiments and previous theoretical calculations.[11, 13, 14] A small induced antiferromagnetic polarization is present in the cell, mostly localized on Ge sites.[11, 13, 14] This is true for all three cases considered. Upon doping, the volume of the unit cell decreases by 1.4 %; the c -axis shrinks faster than the a -axis, thus decreasing the c/a ratio. The M_{II} - M_I separation along the z -axis (*i.e.* $c/2$) affects the length of the c -axis most: the smaller atomic size of Fe compared to Mn (the Fe and Mn covalent radii are 1.25 and 1.39 Å, respectively[12]) is clearly responsible for the contraction of the c -axis upon Fe substitution. Our calculated lattice constants agree well with experimental values.[4, 7] The magnetic

moments at the M_I sites are distributed as follows: Fe carries the lowest magnetic moment ($1.75 \mu_B$), while Mn shows a slightly increased moment compared to pure Mn_5Ge_3 ($2.35 \mu_B$). On the other hand, the M_{II} magnetic moments are only marginally affected by Fe substitution. The experimental values shown in Tab. I are obviously average values for the two independent sublattices: the slight discrepancy between experimental and calculated values could be ascribed to disorder effects which are not taken into account in the present calculation.

It is interesting to explore the $x = 5$ doping limit in the $D8_8$ phase. In the Fe_5Ge_3 phase, there is a significant decrease of the length of both the a - and c -axis by 2.4 and 3.1 % respectively, while the c/a ratio is almost unchanged compared to the $x = 0$ case. The iron magnetic moments decrease to 1.58 and $2.17 \mu_B$ at M_I and M_{II} sublattice, leading to a sizable reduction of the total moment in the cell. Finally, concerning the stability of the compounds, we note that Mn_5Ge_3 and Mn_4FeGe_3 are quite stable (ΔH_f are -0.140 and -0.145 eV/atom respectively), whereas Fe_5Ge_3 has only a slightly negative formation energy (-0.061 eV/atom).

We now focus on the electronic structure of the intermetallic compounds considered. According to Ref. 6, strong metal-germanium and metal-metal covalent bonding is present in this phase. Broad, primarily sp bonding and antibonding bands form due to covalent interactions between Mn and Ge. Since there are three germanium atoms per formula unit, each contributing four orbitals with a spin degeneracy of two per orbital, these bands can accommodate 24 electrons. Assuming formal valences $(Mn,Fe)^{+3}$ at $4(d)$, $(Mn,Fe)^{+2}$ at $6(g)$, Ge^{4-} at $6(g)$, [6] the bonding band is filled with six electrons from the two $4(d)$ metal atoms, six from the three $6(g)$ metal atoms, and twelve from the three metalloid atoms (in total 24). At the Fermi level, a large density of d -like states is present. Therefore, we expect that there will be sheets at the Fermi surface with large and "heavy"-like areas, made up predominantly of electrons relatively localized on partially occupied d -like states and, thus, with large effective masses and low Fermi velocity. On the other hand, there will be also small and "light"-like areas of the Fermi-surface sheets with sp character, made up by highly mobile electrons with delocalized wave functions, small effective masses, and high Fermi velocity. Thus, it is expected that the d -likes state dominate the density of states at the Fermi level, $N(E_f)$, while sp electrons do contribute substantially to the average value of the Fermi velocity.

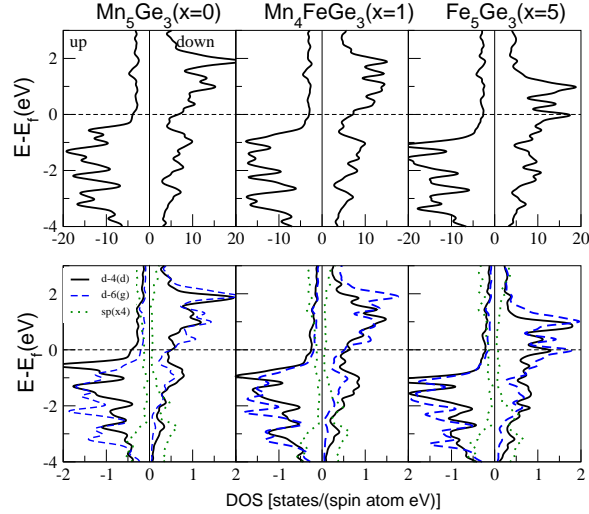


FIG. 1: (color online) Electronic density of states (DOS) of Mn_5Ge_3 , Mn_4FeGe_3 and Fe_5Ge_3 . Total and projected DOS onto metal 4(d) and 6(g) sites are shown in top and bottom panel. The sp -DOS has been multiplied by a factor of 4 for clarity.

Fig. 1 shows the spin resolved total DOS (upper panels) and the DOS projected onto d -states of 4(d) and 6(g) metal atoms as well as onto sp states (lower panels). From left to right, the iron concentration varies from $x=0,1$ to $x=5$. Let us focus on the region around the Fermi level for Mn_5Ge_3 (upper panel): while the spin up DOS has an almost structureless plateau (there is a small valley in the DOS curve just above the Fermi level), the spin down DOS has much more fine structure around and immediately above the Fermi energy. From the lower panel, we see: i) the sp electrons are mainly located in the region below -2 eV (bonding states) and above 1.5 eV (antibonding states), supporting the picture given above; ii) $N(E_f)$ is dominated by d states rather than by sp states, in both spin channels, suggesting that the d electrons are mainly responsible for the spin polarization; iii) the number of sp -electrons with spin-up, N_{sp}^\uparrow , is significantly larger than those with spin-down, N_{sp}^\downarrow , suggesting that the average value of the spin-up Fermi velocity is larger than the corresponding spin-down value.[17] In the majority component, the d -4(d) DOS is larger than the d -6(g) one, while they are practically equal in the minority component. Upon Fe doping (electron-like carrier doping), the Fermi level shifts upwards to accommodate the extra electron per formula unit and now lies at the bottom of the small valley of the majority DOS and on top of a small peak in the minority DOS: as a result, N^\uparrow decreases, and N^\downarrow increases, leading to a more negative spin-polarization P_0 , which is proportional to $N^\uparrow - N^\downarrow$ (see below). These

TABLE II: Spin polarizations for different $x = 0, 1, 5$. See text for further details.

Compound	x_0	y_0^{\parallel}	y_0^{\perp}	$P_0(\%)$	$P_{1\parallel}(\%)$	$P_{1\perp}(\%)$	$P_{2\parallel}(\%)$	$P_{2\perp}(\%)$
Mn_5Ge_3 ($x = 0$)	0.55	2.4	2.1	-30	14	7	52	41
Mn_4FeGe_3 ($x = 1$)	0.28	3.7	2.6	-55	3	-16	59	30
Fe_5Ge_3 ($x = 5$)	0.13	0.5	0.7	-77	-88	-83	-95	-87

modifications are mainly driven by the $d-4(d)$ states and are consistent with a simple rigid band picture. On the other hand, there are negligible changes in N_{sp}^{\uparrow} and N_{sp}^{\downarrow} at E_f .

In the high doping limit, we observe that the majority DOS is hardly modified compared to the lower Fe content case, while the minority component becomes more structured; in fact, the Fermi level is further shifted upwards: it still lies at the bottom of a valley in the majority DOS, while it is pinned at a high peak in the minority component, leading to a very large value of the total DOS at E_f . The large Fe content mainly affects the minority spin DOS and strongly modifies the overall transport properties through large modifications of the minority spin component. As before, the sp -DOS at E_F is marginally affected.

Let us now consider the spin-polarization (SP) of the different compounds. A common definition for SP is:[15]

$$P_n = \frac{N_{\uparrow}(E_F)v_{F\uparrow}^n - N_{\downarrow}(E_F)v_{F\downarrow}^n}{N_{\uparrow}(E_F)v_{F\uparrow}^n + N_{\downarrow}(E_F)v_{F\downarrow}^n} \quad (1)$$

where N and v_F are the density of states (DOS) and average Fermi velocity of electrons with spin-up, spin-down at E_f , respectively. Note that Eq. 1 can be written as follows: $P_n = (x_0 y_0^n - 1)/(x_0 y_0^n + 1)$ with $x_0 = N^{\uparrow}(E_F)/N^{\downarrow}(E_F)$ and $y_0 = v_{F\uparrow}^{\uparrow}/v_{F\downarrow}^{\downarrow}$. Due to the hexagonal symmetry, the Fermi velocity can be decomposed into components which are parallel and perpendicular to the basal plane, $v_{F\parallel}^{\uparrow,\downarrow}$ and $v_{F\perp}^{\uparrow,\downarrow}$ respectively. The same is true for y_0^n .

For $n = 0$, the SP calculated using Eq. 1 corresponds to spin-resolved photoemission measurements, while higher orders of P_n correspond to SP as measured in transport experiments, such as PCAR (point contact Andreev reflection) and TJ (tunnel junction), in the ballistic (P_1) or diffusive regime (P_2).[16] In Tab. II, we show the calculated x_0 and y_0 at E_f for the three compounds, and the corresponding P_n for $n=0,1,2$. Upon iron doping, we see that: i) $N^{\uparrow} < N^{\downarrow}$ (*i.e.* $x_0 < 1$) in all compounds considered and, in particular, $N^{\uparrow} \ll N^{\downarrow}$ for $x = 5$. ii) For both the parallel and perpendicular component, $v_{F\parallel}^{\uparrow} > v_{F\parallel}^{\downarrow}$ (*i.e.* $y_0 > 1$),

except for Fe_5Ge_3 where the opposite is true. The average velocity for spin up v_F^\uparrow is larger than v_F^\downarrow , because the conductivity is dominated by the sp electrons, and in all $\text{Mn}_{5-x}\text{Fe}_x\text{Ge}$ compounds $N_{sp}^\uparrow > N_{sp}^\downarrow$. Fe_5Ge_3 is special, since N_d^\downarrow is exceptionally large (see Fig. 1).

Clearly, point i) leads to negative P_0 , with the absolute values increasing with the Fe content; *i.e.* at the Fermi-level, the spin up density is smaller than the spin down density, and this behaviour is enhanced by Fe doping. However P_1 is greater than P_0 , and P_2 is greater than P_1 , except for Fe_5Ge_3 . This is related to ii), *i.e.* the spin up velocity is exceeds the spin down velocity ($y_0 > 1$) over-compensating the lower spin-up versus spin-down density at Fermi-level. The exception is Fe_5Ge_3 where $y_0 < 1$, and hence P slightly decreases with n ($P_0 \gtrsim P_1 \gtrsim P_2$).

In summary, we have studied the hexagonal phase ($D8_8$) of the $\text{Mn}_{5-x}\text{Fe}_x\text{Ge}$ intermetallic alloy, focusing on the role of the Fe substitution on the structural, electronic and magnetic properties of the compound. We found that: i) Fe substitution preferentially occurs at the $4(d)$ site of the $D8_8$ structure; ii) substitution of one Mn atom/f.u. in Mn_5Ge_3 enhances the spin polarization P_0 in agreement with experiment, but iii) substitution also decreases P_1 and P_2 . The last observation is at variance with the experimental results.[4] The reason for this disagreement deserves further studies that should include disorder as well as interface effects, which are beyond the purpose of the present study. On the other hand, our *ab-initio* calculations indeed confirm that is possible to tune the degree of spin-polarization in the different transport regimes upon Fe doping. Remarkably, an even larger spin polarization than that of Mn_4FeGe_3 can be achieved by further increasing the Fe content, thus making the $\text{Mn}_{1-x}\text{Fe}_x\text{Ge}_3$ intermetallic alloy very promising for future spintronic applications.

Acknowledgments

This work was supported by the Austrian *Fonds zur Förderung der wissenschaftlichen Forschung*; by CNR-INFN through Iniziativa Trasversale Calcolo Parallelo and by Consorzio Gran Sasso through a computing grant at Centro Calcolo dei Laboratori Nazionali del Gran Sasso (INFN).

-
- [1] A. Verdini, A. Cossaro, L. Floreano, A. Morgante, A. Goldoni, D. Ghidoni, A. Sepe, S. Pagliara, and L. Sangaletti, Phys. Rev. B **77**, 075405 (2008).
- [2] C. Zeng, E. Zhu, S. C. Erwin, Z. Zhang, and H. H. Weitering, Phys. Rev. B **70**, 205340(2004).
- [3] A. P. Li, J. Shen, J. Thomspson, and H. Weitering, Appl. Phys. Lett. **86**, 152507 (2005).
- [4] T. Y. Chen, C. L. Chien, and C. Petrovic, Appl. Phys. Lett. **91**, 142505 (2007).
- [5] W. M. Reiff, K.S.V.L. Narasimhan, and H. Steinfink, J. Sol. St. Chem. **4**, 38 (1972).
- [6] V. Johnson, J.F. Weiher, C.G. Frederick, and D.B. Rogers, J. Sol. St. Chem. **4**, 311 (1972).
- [7] J.J. Bara, B.V. Gajič, A.T. Pedziwiatr, and A. Szytula, J. Magn. Magn. Mat. **23**, 149 (1981).
- [8] J. P. Perdew, K. Burke, and M. Ernzerhof, Phys. Rev. Lett. **77**, 3865 (1996).
- [9] P. E. Blöchl, Phys. Rev. B **50**, 17953 (1994).
- [10] G. Kresse, and D. Joubert, Phys. Rev. B **59**, 1758 (1999).
- [11] S. Picozzi, A. Continenza, and A.J. Freeman, Phys. Rev. B **70**, 235205 (2004).
- [12] www.webelements.com
- [13] J.B. Forsyth, and P.J. Brown, J. Phys.: Condens. Matter **2**, 2713 (1990).
- [14] A. Stroppa, and M. Peressi, Phys. Status Solidi (a) **204**, 44 (2006).
- [15] I.I. Mazin, Phys. Rev. Lett. **83**, 1427 (1999).
- [16] M.S. Bahramy, P. Murugan, G.P. Das, and Y. Kawazoe, Phys. Rev. B **75**, 054404 (2007).
- [17] Remember that *sp*-electrons are expected to have large velocity.